Phase Distribution during Isothermal Crystallization of Polyethylene Probed by Solid-State Proton NMR Free Induction Decay

Per Eugen Kristiansen,*,† Eddy Walther Hansen,‡ and Bjørn Pedersen†

Department of Chemistry, University of Oslo, P.O. Box 1033, Blindern, 0315 Oslo, Norway, and SINTEF Applied Chemistry, P.O. Box 124 Blindern, 0314 Oslo, Norway

Received: November 30, 1998

Solid-state proton NMR free induction decay (FID) during isothermal (394 K) crystallization from a molten polyethylene sample has been investigated. On the basis of deconvolution of the FID signal, three different phases are assigned and their relative distribution during crystallization determined. The results are discussed in light of the Avrami model. The formation of the crystalline phase during the primary crystallization time regime increases approximately with the square root of crystallization time. Kinetic data regarding the crystallization process are obtained and discussed.

Introduction

It is well-known that crystallization and processing of a polymer will affect its morphology.[1,2] In particular, much effort has been exercised to understand the effect of crystallization on morphology,[2−6] as this may affect the physical properties of the polymer.[7] Having once established that certain polymeric materials are capable of crystallization, fundamental studies related to the mode and kinetics of crystallization have been reported.[2,8−10] The most common experimental techniques used to characterize the crystallization process have been dilatometry,[2,8−10] X-ray diffraction,[11] light polarization,[12] and optical microscopy.[13] Dilatometry and optical methods monitor the change in density and size of the growing nuclei, respectively.

NMR spectroscopy has shown that at least three phases are involved in the crystallization process and that the degree of crystallinity is dependent on the preparation of the polymer.[3,4,14,15] These results suggest that NMR is a powerful tool for characterizing polymer morphology and, in particular, for distinguishing between different phases formed during crystallization. To the best of our knowledge, no in situ NMR studies on isothermal crystallization of polyethylene have been reported.

Dadayli et al.[16], Hansen et al.,[17] and Kristiansen et al.[18] have recently reported a promising method for determining the crystallinity of polypropylene and polyethylene from solid-state proton NMR. In particular, they showed that analysis of the frequency NMR spectrum of polyethylene resulted in a systematic underestimate of crystallinity compared to a direct analysis of the FID. This discrepancy originates from the obligatory blanking time of the receiver to avoid rf-pulse breakthrough.[17] While Dadayli et al.[16] and Hansen et al.[17] determined crystallinity at room temperature, Kristiansen et al.[18] showed that the same NMR technique could be used to analyze the crystallinity of polyethylene at any temperature below its melting point.

With this in mind we found it appealing to apply this solid-state proton NMR "FID analysis technique" to monitor the crystallinity and potential phase changes during an isothermal crystallization process, in situ. Also, molecular motional characteristics of the different phases, as well as the mathematical−physical model used to analyze the FID, will be addressed.

In short, the main object of the present work is to evaluate the potential use of the "NMR FID analysis technique" in characterizing the crystallization processes of polyethylene (and other polyolefins).

Experimental Section

Material. The polyethylene (PE) sample investigated in this work was received from Borealis AS. The sample contained only butyl branches (4−5 per 1000 main chain carbons), which was determined from high-resolution ^{13}C NMR.[18] The sample Mw is 66 000 g/mol, and since it is a single-site polymer, the molecular weight distribution is narrow.

The polyethylene sample was initially kept at 413 K for 30 min within the NMR magnet to ensure that all of the polymer was melted (melting point of the received sample was approximately 396 K). The sample was then cooled to 400 K for 10 min before being cooled to 394 K, at which temperature all the NMR FIDs were acquired. The time of the last temperature change (from 400 to 394 K) was defined as zero time.

NMR. All NMR measurements were performed on a Bruker DMX 200 AVANCE instrument operating at a 200 MHz proton resonance frequency. A high-power ^1H NMR probe capable of producing 90° radio frequency (rf) pulses of approximately 1.5 μs was used. The FID was sampled every 0.2 μs. To avoid pulse breakthrough, a receiver blanking time ("dead time") of 2 μs was applied. One scan was acquired in each experiment, and a total of 200 experiments were performed. The time delay between each experiment was initially set to 15 s, which is much longer than 5 times the longer spin−lattice relaxation time T_1 (<1.5 s) of the methylene protons and ensures quantitative sampling of the FID. This time delay was increased twice during the experiment to 75 and 625 s, respectively. The actual phase parameters were adjusted manually to give a pure absorption spectrum in order to ensure that only the real part of the FID was sampled.

Each FID was sampled for 4.4 ms, resulting in 22K of data points. Before transferring the data to a PC for processing, the data matrix was reduced in size by selecting each of the 200

* To whom correspondence should be addressed.
† University of Oslo.
‡ SINTEF Applied Chemistry.

10.1021/jp984539j CCC: $18.00
Published on Web 04/20/1999

sampled data points from 2 to 42 μs and 500 data points from 42 μs to 4.4 ms (every 44th point of the residual part of the FID). This particular selection of data points, from 22 to 0.7 K, was favored by visual inspection of all the sampled FIDs, simultaneously. The reason for performing such a data reduction or filtering was to speed up the subsequent calculation (on a PC) when using the program "solver" in Microsoft Excel.

The temperature within the probe was calibrated by use of an NMR thermometer of ethylene glycol and controlled by a Bruker B-VT2000 unit. The actual temperature was estimated to be stable and accurate to about $\pm$0.5 K.

Theoretical Outline

A detailed discussion of how to analyze the solid-state proton NMR FID of polyethylene has been reported resently,[17,18] so only a brief description will be given here.

Crystalline Phase. From an NMR point of view, PE represents a rather "simple" polymer system in which the two-proton nuclei of each methylene group constitute a strong dipole−dipole coupled two-spin system. Owing to the weaker dipole−dipole coupling between protons on different methylene groups, the absorption line shape function of the protons in PE can be considered, to a good approximation, to arise from a Gaussian broadened two-spin interaction, where the broadening is due to the other neighbors. Pake[19] derived an analytical expression for such an absorption spectrum of coupled spin $^1/_2$ nuclei. However, owing to the inherent NMR dilemma related to rf-pulse breakthrough,[20] the theoretical Pake function cannot be fitted directly to the frequency spectrum. Rather, we need to obtain the inverse Fourier transform of the Pake expression, which will represent the observed signal intensity in the time domain. Look and co-workers[21] presented an analytical solution to this enigma, which has been used recently by Hansen et al.[17] and Kristiansen et al.[18]

$$P(t) = \sqrt{\frac{\pi}{6}} \exp\left[-\frac{1}{2}\beta^2 t^2\right]\left\{\frac{\cos \alpha t}{\sqrt{\alpha t}} C\left[\sqrt{\frac{6\alpha t}{\pi}}\right] + \frac{\sin \alpha t}{\sqrt{\alpha t}} S\left[\sqrt{\frac{6\alpha t}{\pi}}\right]\right\} \quad (1a)$$

where $P(t)$ defines the normalized time-dependent FID and $C[x]$ and $S[x]$ are the so-called Fresnell functions, which are defined as simple integral equations.[22] The parameter α is related to the distance, R_{H-H}, between the two nearest-neighbor protons of the methylene group,

$$\alpha = \frac{3\gamma^2\hbar}{4R_{H-H}^3} \quad (1b)$$

where γ is the nuclear gyromagnetic ratio and $\hbar$ is Planck's constant. β represents the width of the Gaussian broadening function, which takes account of dipole−dipole interactions between protons on different methylene groups. To apply eq 1 as a fitting function, a more tractable form of the Fresnel functions is needed. The following approximations have been used:[22]

$$C(x) = \frac{1}{2} + f(x)\sin\left[\frac{\pi}{2}x^2\right] - g(x)\cos\left[\frac{\pi}{2}x^2\right] \quad (1c)$$

$$S(x) = \frac{1}{2} - f(x)\cos\left[\frac{\pi}{2}x^2\right] - g(x)\sin\left[\frac{\pi}{2}x^2\right] \quad (1d)$$

where

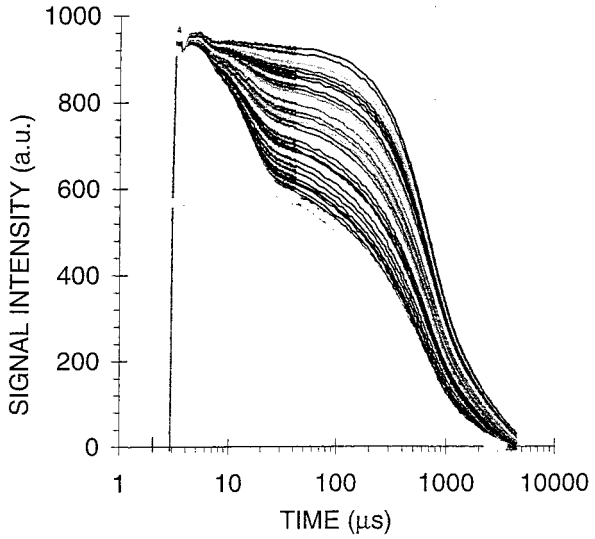

Figure 1. Observed ^{1}H-FIDs of polyethylene during isothermal crystallization at 394 K. The FIDs are acquired at the following times (minutes): 6.5, 9, 11.5, 12.5, 13, 13.5, 14, 15, 15.5, 16, 16.5, 17, 17.75, 19, 19.5, 20.25, 21.5, 22.75, 21.5, 22.75, 24, 25, 26, 26.5, 29, 31.5, 34, 39, 44, 50, 75 (from top to bottom).

$$f(x) = \frac{1 + 0.926x}{2 + 1.792x + 3.104x^2} + \epsilon(x) \quad (1e)$$

$$g(x) = \frac{1}{2 + 4.142x + 3.492x^2 + 6.670x^3} + \epsilon(x) \quad (1f)$$

The absolute error, $\epsilon(x)$, in these approximations is less than 2×10^{-3}.

Amorphous Phase. In contrast to the crystalline phase of PE, the amorphous phase is evidenced by an increased fluctuation in the molecular mobility, which is expected to modify the shape of the NMR spectrum. Brereton et al.[23,24] have derived an exact, theoretical expression for the FID of a dynamic scale invariant polymer chain governed by a single relaxation time. The function has been successfully applied as reported in a recent investigation of PE at room temperature.[17] Dadayli et al.[16] have pointed out that the rather complex "Brereton" function can be well approximated by the sum of a Weibullian function, $W(t)$, and one or two exponential functions:

$$W(t) = \exp\left[-\left(\frac{t}{T_{2c}}\right)^n\right] \quad (2)$$

The normalized Weibullian function ranges between a pure Lorentzian ($n = 1$) and a pure Gaussian ($n = 2$). It should be emphasized, however, that there is no direct theoretical justification for the approximation of a "Brereton" function to a sum of a Weibullian and one or two exponential functions. This approximation is basically an empirical one.

Results and Discussion

FID of Polyethylene during Isothermal Cooling. Figure 1 shows a series of free induction decays (FIDs) of a melted polyethylene (PE) sample as a function of time. The FIDs are acquired immediately after the sample is placed into the NMR magnet at a setting temperature of 394 K. The shape of the FID changes with time because of an uninterrupted crystallization process. The formation of a crystalline phase is recognized by the relative increase of a fast decaying component ($t < 20$ μs) of the FID with increasing reaction time. To obtain

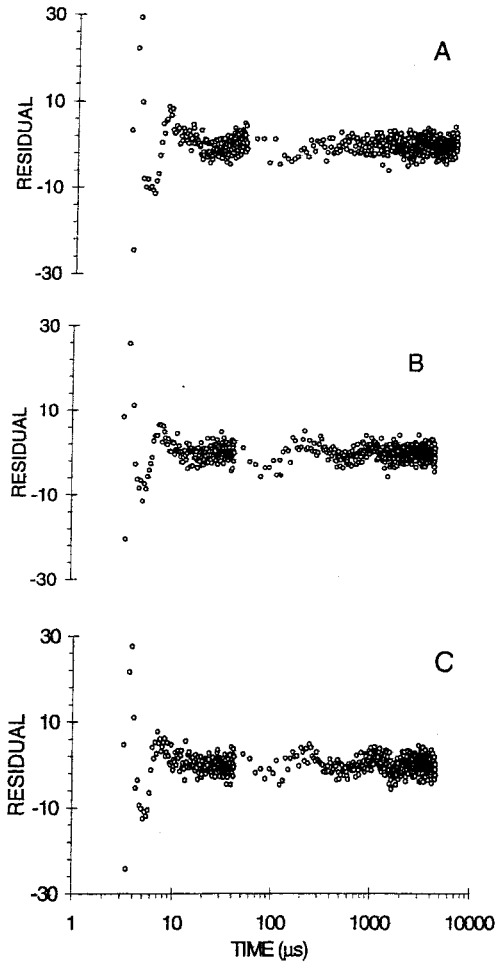

Figure 2. Residuals between observed and model-fitted FIDs at three different times during crystallization: (A) $t = 14$ min; (B) 25 min; (C) 444 min. See text for further details.

quantitative information regarding this crystalline phase, each FID was fitted to a theoretical model represented by a sum of a Pake function (eq 1), a Weibullian function (eq 2), and two exponential functions (eq 2; $n = 1$), as outlined in a previous section. In this work we will use a shorthand notation *P*, *W*, and *E* for these different types of function. The actual combination of these functions will be simply referred to as the "PWEE" (Pake−Weibullian−exponential−exponential functions) model. A more extensive discussion on this topic can be found in recent published studies.[17,18]

The relatively small residuals, i.e., the difference between observed and model-fitted FIDs, at three different crystallization times are shown in Figure 2 and reveal approximately random error distribution curves. The larger residuals observed for $t <$ 4−5 μs are due to breakthrough of the rf pulse and are excluded from the model fits. The parameters α and β (in eq 1), which uniquely define the crystalline part of the FID, are assumed to be constant and independent of temperature. Also, the spin−spin relaxation time (T_2) of the fast-decaying exponential function E_1 was assumed to be constant and independent of crystallization time. These parameters may vary slightly with time, as suggested in a recent study.[18] However, owing to the very small amount of crystalline and intermediate phases formed at the early stage of the crystallization process, these three parameters cannot be reliably determined by the curve-fitting analysis for short crystallization times. On this ground, we decided to keep these parameters constant and equal to their values determined for longer reaction times. Indeed, at longer

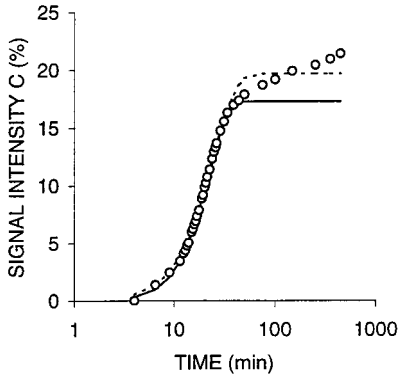

Figure 3. Signal intensity of the Pake component of the FID (crystalline phase) as a function of crystallization time. The solid and dotted curves represent model fits to eq 3b for times $0 < t < t_d$ (=37 min) and for $0 < t < 400$ min, respectively.

crystallization times, these parameters were found to be, within experimental uncertainty, constant and equal to $\alpha = 1.15 \times 10^5$ s^{-1}, $\beta = 3.86 \times 10^4$ s^{-1}, and $T_2 = 26$ μs, respectively. Approximately the same numbers were reported in nonisothermal investigations of the same polymer sample.[21]

"Two-Stage" Crystallization. As previously pointed out, the percent contribution to the FID of the different components *P*, *W*, and *E* of the "PWEE" model can be obtained by a nonlinear least-squares technique. As will become clear later (see also refs 17 and 18), the *P* component of the FID can be uniquely assigned to the crystalline phase (C). The relative amount of this phase changes with time as shown in Figure 3. To model this behavior, we have applied eq 3

$$\theta_X(t) = \theta_{X\infty} - (\theta_{X\infty} - \theta_{X0}) \exp[-(kt)^\beta] \qquad (3a)$$

where θ_{X0} represents the amount of phase X at time $t = 0$, $\theta_{X\infty}$ represents the amount of phase X at infinite time, and k and β represent adjustable parameters. For any phase X, which is zero ($\theta_{X0} = 0$) at the start of the reaction ($t = 0$), eq 3 simplifies to

$$\theta_X(t) = \theta_{X\infty}[1 - \exp(-[kt]^\beta)] \qquad (3b)$$

which is equivalent to the well-known Avrami equation.[25,26] The terms k and β represent the rate constant and the Avrami exponent, respectively. The former parameter depends on the nucleation and growth rates, while the latter depends on the nature of nucleation, polymer transport to the growing crystal, and growth geometry.

The dotted curve in Figure 3 represents a nonlinear least-squares fit of the Avrami equation (eq 3b) to the observed data within the whole time regime and gives a rather poor fit for times larger than approximately 30−40 min. When the Avrami equation (eq 3b) is fit to the initial data points ($t < 40$ min), a solid curve arises, which also reveals a correspondingly poor fit for times $t > 40$ min.

These results give support for a two-stage crystallization process to occur, which has recently been proposed and discussed by Eamor et al.[27] in a study on the crystallization of poly(butylene terephthalate) and by Banks et al.[10] in their study of polyethylene. To describe such a two-stage process they applied a two-step function composed of two time functions in series. The primary crystallization, though progressing at a much decelerated rate in the later stage, still continues in parallel to the secondary crystallization that starts in series at a certain time $t = t_d$. If the mass fraction undergoing secondary crystallization is represented by the function $L(t)$, the following generalized

TABLE 1: Parameters θ_0, θ_{A0}, θ_{A1}, k, β, C_0, and C_1 in Eqs 1, 2, and 4 Obtained by a Nonlinear Least-Squares Fit to the Observed NMR Signal Intensities in Figure 5

parameter	P	E_1	W	E_2
A_X	-5.84 ± 0.14	-0.12 ± 0.01	6.60 ± 0.15	0.67 ± 0.02
B_X	1.64 ± 0.04	0.48 ± 0.02	-1.86 ± 0.05	-0.14 ± 0.01
k (min^{-1})	$(4.56 \pm 0.09) \times 10^{-2}$	$(4.94 \pm 0.02) \times 10^{-2}$	$(4.38 \pm 0.07) \times 10^{-2}$	$(5.69 \pm 0.02) \times 10^{-2}$
β	2.33 ± 0.07	3.23 ± 0.03	2.38 ± 0.03	3.74 ± 0.02
θ_{X0}	0	0	54.3 ± 1.6	46.7 ± 1.2
$\theta_{X\infty}$	17.28 ± 0.84	18.31 ± 0.19	23.1 ± 0.6	39.4 ± 1.0

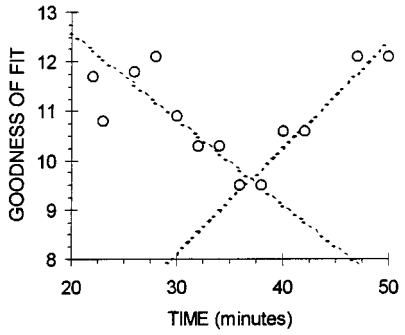

Figure 4. "Goodness of fit" obtained by model fit of eq 3 to the observed "phase" concentrations by different values of the time parameter t_d.

equation, $\psi(t)$, predicts the mass fraction of phase X at any time t during the crystallization process:

$$\Psi_X(t) = \theta_X(t) + L_X(t) \tag{3c}$$

From the observed time evolution of crystallization at longer times (Figure 3; $t > 40$ min), the following empirical function, $L_X(t)$, was chosen:

$$L_X(t) = 0 \qquad t < t_d$$
$$= A_X + B_X \ln(t) \qquad t \geq t_d \tag{3d}$$

where A_X and B_X are constants. Such a logarithmic time evolution of the secondary crystallization process has been previously proposed and applied by Ergoz et al.[28] from density measurements of PE.

To obtain a reliable value of the time parameter t_d in eq 3d, this equation was fitted simultaneously to the observed signal intensities P, W, and E of the "PWEE" model for different values of t_d. The standard error of estimate, denoted the "goodness of fit", is plotted in Figure 4 versus t_d. This plot shows a minimum value for the "goodness of fit" parameter for t_d of approximately 37 min. Since the signal intensities are acquired at discrete times during the crystallization process, t_d can only be estimated to within the time interval $35 < t_d < 40$ min. The numerical values of the fitted parameters (eq 3) for all components are summarized in Table 1. The solid curves in Figure 5 represent the best model fits to eq 3 with $t_d = 37$ min. Figure 5 (bottom) shows the residuals of the model fit and suggests that the error is randomly distributed. This observation was used to estimate the uncertainty in the derived parameters (eq 3, Table 1) according to a procedure outlined in ref 29.

Assignment of Phases. Spin−Spin Relaxation Times. The spin−spin relaxation time (T_2) of the W and E components of the "PWEE" model is uniquely defined by eq 2. One of the two single-exponential functions (E_1) shows a spin−spin relaxation time that is, within experimental error, constant and independent of crystallization time. The short relaxation time of approximately 26 μs suggests that these molecules have a rather restricted mobility. This FID component is tentatively

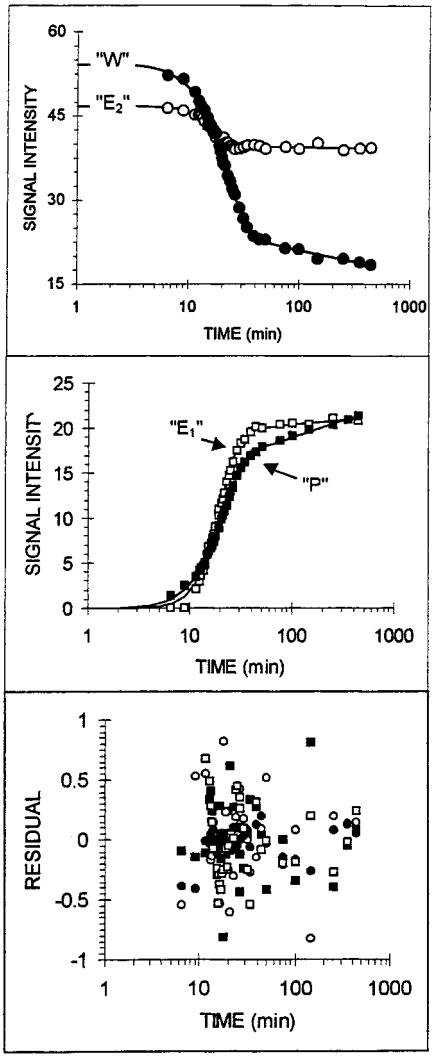

Figure 5. Signal intensity versus reaction time of the four FID components W, E_2 (top), and E_1, P (middle). The solid curves represent model fits to eqs 3. The bottom figure shows the residual between observed and model-fitted signal intensities

assigned to an intermediate phase I. It needs to be emphasized, however, that part of this signal intensity may originate from an increased internal segmental motion within the crystalline phase. Since increasing mobility will result in an increasing T_2, such a motional effect may accidentally result in a T_2 component that is about the same as observed for the intermediate phase.

The two other components W and E_2 of the "PWEE" model reveal significantly longer spin−spin relaxation times (Figure 6). The solid curves in Figure 6 are nonlinear least-squares fits to eq 3 (with Ψ, θ, and L replaced by $1/T_2$) and represent the observed relaxation data surprisingly well—surprisingly, in the sense that, to the best of our knowledge, no known theoretical model for describing the time evolution of the spin−spin relaxation rate, $1/T_2$, has ever been reported. In this work, we simply consider this model fit as an empirical fit.

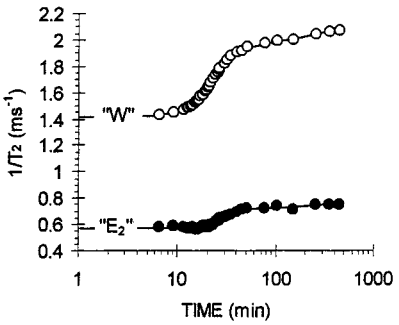

Figure 6. Spin−spin relaxation rate ($1/T_2$) vs crystallization time of components W and E_2. The solid curves represent model fits to eq 3 (with Ψ, θ, and L replaced by $1/T_2$). See text for further details.

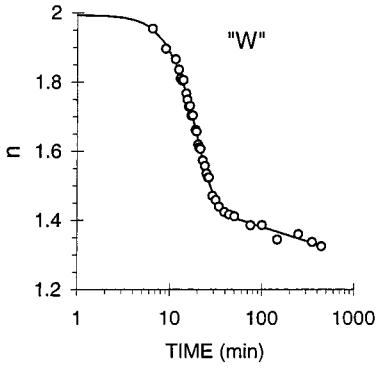

Figure 7. Exponent n (eq 2) vs crystallization time. The solid curve represents model fit to eq 3 (with Ψ, θ, and L replaced by n). See text for further details.

Also, the time evolution of the parameter n of the Weibullian function (eq 2) could be excellently fitted to eq 3 (Figure 7) and suggests that this equation may be of a more general validity than simply accounting for the time evolution of the crystalline amount only. These observations merit a more fundamental and theoretical approach concerning the analysis of the time evolution of the spin−spin relaxation rate of the different phases involved during the crystallization process. However, this subject is outside the scope of this work.

The physical reason for deriving an n-value of the Weibullian (W) function (eq 2) different from 1 or 2 is somewhat controversial, However, one frequently used interpretation is that a distribution of relaxation times exist. In particular, the n parameter is seen (Figure 7) to drop from approximately 2 (Gaussian) at the early part of the crystallization process toward a value somewhat larger than 1 (Lorenzian) during the primary crystallization time regime. According to the above discussion, this observation suggests that the distribution characteristics of T_2 changes with crystallization time.

On the basis of the work by Bremner et al.[30] and Brereton et al.[24] that the amorphous phase of PE was described by more than a single FID component, the W and E_2 components of the FID were assigned to the amorphous phase. Recently, Bremner et al. assigned the different FID components to amorphous low-molecular weight material (nonnetwork fraction), amorphous entangled network fraction, and an ordered or high segmental-density fraction in order of decreasing relaxation times. One objection to the above assignment of the FID components is that one of the components E_2 or W may belong to the intermediate phase I. However, this would lead to an estimated relative amount of the intermediate phase that is physically unrealistic. Also, the T_2 of these components are significantly larger than that expected for a more restricted (inter)phase.[18]

An additional and indirect support for the above assignment was the time dependence of the average spin−spin relaxation rate ($1/T_{2,\mathrm{av}}$) of the amorphous phase. Although such an average value cannot be unambiguously defined, we adopted the conventional and often applied definition of a "weighted" average, eq 4:

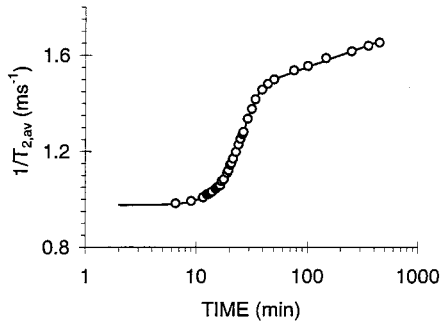

Figure 8. Average spin−spin relaxation rate ($1/T_{2,\mathrm{av}}$; eq 4) of the amorphous phase vs crystallization time. The solid curve represents model fit to eq 3 (with Ψ, θ, and L replaced by $1/T_2$). See text for further details.

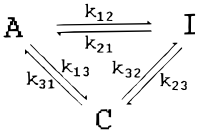

Figure 9. Generalized reaction scheme for a three-phase system. k_{ij} represents rate constants.

$$(W + E_2)\frac{1}{T_{2,\mathrm{av}}} = W\frac{1}{T_{2,W}} + E_2\frac{1}{T_{2,E_2}} \qquad (4)$$

where W and E_2 represent the observed relative signal intensities of the FID components W and E_2 (Figure 5). The results are shown in Figure 8, where the solid curve is calculated by a nonlinear least-squares fit to eq 3. $T_{2,W}$ and T_{2,E_2} were taken from Figure 6.

Concerning the Pake function, which uniquely describes the crystalline phase (C), no explicit T_2 can be defined. However, an approximate value of the spin−spin relaxation time of this phase can be estimated by defining T_2 as the time at which the FID reaches 1/e of its initial value ($t = 0$)[31] and gives $T_2 \approx 12.5$ μs.

It is generally expected that a growth geometry of spherulites will give a value 3 for the Avrami exponent (β; eq 3b), while a value of $\beta = 2$ would signify a growth geometry of disk shapes. As can be seen from the data in Table 1, the Avrami exponent (β) of the crystalline phase is closer to 2 than 3. However, as pointed out by Strobl et al.,[32] one should be careful in putting too much emphasis on the crystalline morphology based on the derived β value.

A number of similar NMR isothermal crystallization experiments (at different temperatures) have been initiated in this laboratory and will be reported in the near future, aiming at clarifying these subtleties. It is our intention to combine such NMR experiments with other methods. At present, we will thus not put too much emphasis on the derived β value but simply use the Avrami equations as empirical fitting functions in order to discuss the phase dynamics during the crystallization process.

Crystallization Dynamics. From the results presented in the previous sections, we aimed at designing a dynamic reaction model between phases by starting with a rather generalized reaction scheme, as presented in Figure 9. Assuming a first-order reversible reaction, the following differential equations can be derived:

$$\frac{dA}{dt} = -(k_{12} + k_{31})A + k_{21}I + k_{13}C \quad (5a)$$

$$\frac{dI}{dt} = -(k_{13} + k_{21})I + k_{12}A + k_{32}C \quad (5b)$$

$$\frac{dC}{dt} = -(k_{32} + k_{13})C + k_{31}A + k_{23}I \quad (5c)$$

When all k_{ij} were assumed to be constant and independent of reaction time, it was not possible to obtain an acceptable fit (within experimental error) to the observed data points, suggesting that the proposed reaction model is not of first order with respect to the different phases. Another reason for the difficulty in fitting this model to the observed intensity data may be that the tentatively assigned intermediate phase contains a contribution from the crystalline phase, as discussed in a previous section. On this ground we tested the following simplified reaction model, which has the additional effect of improving the numerical stability. Also, to avoid introducing reaction order parameters, we decided to implement them into the "rate constants" k_{ij}, thus making these parameters time-dependent. This approach is equivalent to considering the following simplified reaction scheme:

$$A \underset{k'_{21}}{\overset{k'_{12}}{\leftrightarrow}} C \quad (6a)$$

where C represents the total amount of nonamorphous phase, defined by the sum of I and C (C = I + C). This gives the following differential equation:

$$\frac{dA}{dt} = -k' \quad (6b)$$

There are, however, too few experimental data points available to obtain reliable estimates of the time dependence of k'_{12} and k'_{21}. Noting, however, the excellent model fits obtained for the "phases" A and C (Figure 10), the following procedure was applied.

At any time t_i during the crystallization process, 400 time points were chosen within a time interval $t_i + \Delta_i/2$ where Δ_i was defined so that the concentration of A (or C) did not change by more than a few percent within this time interval. The corresponding 400 concentrations of A and C and their time derivatives were calculated from the previously obtained model fits (Figure 10). Assuming k'_{12} and k'_{21} to be constant within these small time intervals (Δ_i), these "rates" were determined from eq 6b by applying a simplex algorithm. These calculated rates are presented in Figure 11(top) as a function of reaction time t. Also, the ratio between the two rates k_{12}/k_{21} is plotted in Figure 11 (bottom). As can be inferred from Figure 11 (top), these rates can be well approximated by simple power laws for times up to approximately $t = t_1 \approx 20$ min, i.e., $k'_{12} = 1.13t^{1.17}$ and $k'_{21} = 0.010t^{0.90}$. The time t_1 corresponds rather well with the time at which the rate of formation of C reaches a maximum, i.e.,

$$t_1 = \frac{1}{k}\left[\frac{\beta - 1}{\beta}\right]^{1/\beta} = 17.6 \text{ min}$$

from eq 3b. Above $t = t_1$, the two rates reach their maximum value at approximately $t = t_2$. Above this latter time, the rates drop dramatically to $t = t_3$. Within the time interval $t_1 - t_3$, the ratio k_{12}/k_{21} is approximately constant and independent of reaction time. It is worth noting that t_2 and t_3 correspond to the times at which the second crystallization process is initiated and the time at which the primary crystallization process is ended, respectively. For times $t > t_3$, the two rates may again be described by simple power laws in time, i.e., $k'_{12} = 0.030t^{-0.97}$ and $k'_{21} = 0.007t^{-1.05}$.

The small difference in exponents between these two rates suggests that a dynamic equilibrium between the two phases is not yet obtained, even at time $t = 400$ min (400 min represent the last measurement performed in this work).

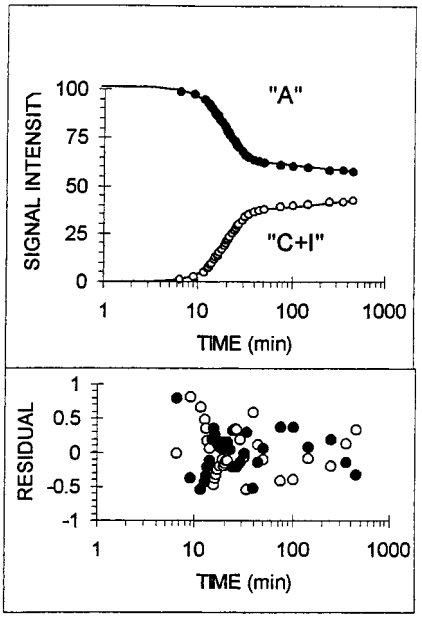

Figure 10. (Top) Signal intensities of amorphous phase (A) and nonamorphous phase C = (C + I) vs crystallization time. (Bottom) Residual between observed and model-fitted signal intensities. See text for further details.

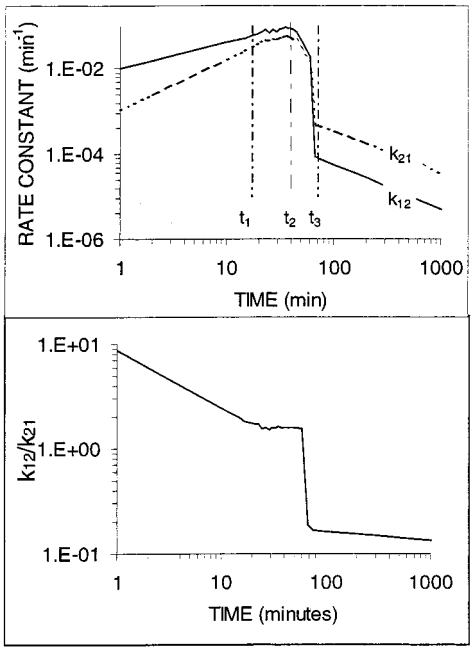

Figure 11. (Top) Calculated rates k_{12} and k_{21} vs crystallization time for the simplified reaction $A \leftrightarrow C$ (eq 6a) as obtained by fitting eq 6b to the model-fitted signal intensities Figure 10. (Bottom) k_{12}/k_{21} vs crystallization time. See text for further details.

Conclusion

In situ solid-state proton NMR free induction decay (FID) analysis of a PE sample during isothermal crystallization at 394

K enables the relative distribution of the different phases (crystalline, amorphous, intermediate) to be monitored as a function of crystallization time. Owing to a potential onset of internal segmental motion within the crystalline phase at this high temperature, part of the crystalline intensity may contribute to the signal intensity of the intermediate phase. The intermediate phase at very high temperature may thus be somewhat ambigiously defined.

The time development of the different phases can be well modeled by an extended Avrami model equation, enabling the transition time between the primary and secondary crystallization regimes to be extracted. Of particular novelty, the time dependence of the spin−spin relaxation rate of the amorphous phase can be excellently described by an extended Avrami model function, which presents some new theoretical challenges.

Furthermore, the in situ NMR measurements enables kinetic information on the crystallization process to be extracted. For instance, a rather dramatic reduction in the rate of formation of the crystalline phase occurs at the transition zone between the primary and secondary time regime.

In short, the present NMR method has the potential of acquiring information on the phase distribution and kinetics of polymer crystallization, in situ. Corresponding isothermal crystallization experiments on PE samples at different crystallization temperatures are in progress.

Acknowledgment. We are grateful to Borealis AS for making the PE samples available for NMR characterization.

References and Notes

(1) Mandelkern, L. *Crystallization of polymers*; Dosier, M., Ed.; Kluwer Academic Publishers: The Netherlands, 1993; pp 25−37.

(2) Ergoz, E.; Fatou, J. G.; Mandelkern, L. *Macromolecules* **1972**, *5*, 147−157.

(3) Kitamaru, R.; Horii, F. *Adv. Polym. Sci.* **1978**, *26*, 137−178.

(4) Kitamaru, R.; Horii, F.; Murayama, K. *Macromolecules* **1986**, *19*, 636−643.

(5) Chen, J.; Fone, M.; Reddy, V. N.; Schwartz, K. B.; Fisher, P. H.; Wunderlich, B. *J. Polym. Sci., Part B: Polym. Phys*. **1994**, *32*, 2683−2693.

(6) Kitamaru, R.; Horii, F.; Zhu, Q.; Basset, D. C.; Olley, R. H. *Polymer* **1994**, *35*, 1171−1181.

(7) Boyd, R. H. *Polym. Rev.* **1985**, 323−447.

(8) Rybnikar, F. *J. Polym. Sci.* **1960**, *44*, 517−522.

(9) Buckser, S.; Tung, L. H. *J. Phys. Chem*. **1959**, *63*, 763−765.

(10) Banks, W.; Gordon, M.; Roe, R.-J.; Sharples, A. *Polymer* **1963**, *4*, 61−74.

(11) Schultz, J. M.; Robinson, W. H.; Pound, G. M. *J. Polym. Sci., Part A-2* **1967**, *5*, 511−533.

(12) Flory, P. J.; McIntyre, A. D. *J. Polym. Sci.* **1955**, *18*, 592−594.

(13) Lambert, W. S.; Phillips, P. J. *Polymer* **1996**, *37*, 3585−3591.

(14) Chen, J.; Fone, M.; Reddy, V. N.; Schwartz, K. B.; Fisher, P. H.; Wunderlich, B. *J. Polym. Sci., Part B: Polym. Phys.* **1994**, *32*, 2683−2693.

(15) Kitamaru, R.; Horii, F. *Adv. Polym. Sci*. **1978**, *26*, 137−178.

(16) Dadayli, D.; Harris, R. K.; Kenwright, A. M.; Say, B. J.; Sunnetcioglu, M. M. *Polymer* **1995**, *35*, 4083

(17) Hansen, E. W.; Kristiansen, P. E.; Pedersen, B. *J. Phys. Chem.* **1998**, *102*, 5444−5450.

(18) Kristiansen, P. E.; Hansen, E. W.; Pedersen, B. *Polymer*, submitted.

(19) Pake, G. E. *J. Chem. Phys.* **1948**, *16*, 327.

(20) Engelsberg, M.; Lowe, I. J. *Phys. Rev.* **1974**, *10*, 822.

(21) Look, D. C.; Lowe, I. J.; Nortby, J. A. *J. Chem. Phys.* **1966**, *44*, 3441.

(22) Abramowitz, M.; Stegun, I. *Handbook of Mathematical Functions*; Dover: New York, 1970; pp 300−303.

(23) Brereton, M. G. *J. Chem. Phys.* **1991**, *94*, 2068.

(24) Brereton, M. G.; Arden, I. M.; Boden, N.; Wright, P. *Macromolecules* **1991**, 24, 2068.

(25) Avrami, M. *J. Chem. Phys.* **1939**, *7*, 1103.

(26) Avrami, M. *J. Chem. Phys.* **1940**, *8*, 812.

(27) Woo, E. M. W.; Yau, S. N. *Polym. Eng. Sci.* **1998**, *39*, 583−589.

(28) Ergoz, E.; Fatou, J. G.; Mandelkern, L. *Macromolecules* **1995**, *28*, 5827.

(29) Hansen, E. W.; Gran, H. C.; Kvernberg, P. O.; Pedersen, B. *J. Phys. Chem. B* **1997**, *101*, 9206−9214.

(30) Bremner, T.; Rudin, A. *J. Polym. Sci., Part B: Polym. Phys*. **1992**, *30*, 1247.

(31) Bjorkstam, J. L.; Listerud, J. *J. Magn. Res*. **1985**, *65*, 383−394.

(32) Strobl, G. R. In *The Physics of Polymers*, 2nd ed.; Springer-Verlag: Berlin, 1997; p 160.